The Fractalline Properties of Experimentally Simulated PWR Fuel Crud

The Fractalline Properties of Experimentally Simulated PWR Fuel Crud

I. Dumnernchanvanit[a], V. K. Mishra[b], N. Q. Zhang[c], S. Robertson[a], A. Delmore[a], G. Mota[a], D. Hussey[d], G. Wang[e], W. A. Byers[e], M. P. Short[a,*]

[a]*Dept. of Nuclear Science and Engineering, Massachusetts Institute of Technology (MIT), 77 Massachusetts Ave., Cambridge, MA, 02139, USA*
[b]*Dept. of Mechanical Engineering, University of Arkansas, Fayetteville, AR, 72701, USA*
[c]*Key Laboratory of Condition Monitoring and Control for Power Plant Equipment of Ministry of Education, North China Electric Power University (NCEPU), Beijing 102206, China*
[d]*Electric Power Research Institute (EPRI), 3420 Hillview Ave, Palo Alto, CA, 94304, USA*
[e]*Westinghouse Electric Company, 1332 Beulah Road, Pittsburgh, PA, 15235, USA*

Abstract

The buildup of fouling deposits on nuclear fuel rods, known as crud, continues to challenge the worldwide fleet of light water reactors (LWRs). Crud may cause serious operational problems for LWRs, including axial power shifts, accelerated fuel clad corrosion, increased primary circuit radiation dose rates, and in some instances has led directly to fuel failure. Numerous studies continue to attempt to model and predict the effects of crud, but each makes critical assumptions regarding how to treat the complex, porous microstructure of crud and its resultant effects on temperature, pressure, and crud chemistry. In this study, we demonstrate that crud is indeed a fractalline porous medium using flowing loop experiments, validating the most recent models of its effects on LWR fuel cladding. This crud is shown to match that in other LWR-prototypical facilities through a porosity-fractal dimension scaling law. Implications of this result range from post-mortem analysis of the effects of crud on reactor fuel performance to utilizing crud's fractalline dimensions to quantify the effectiveness of anti-fouling measures.

1. Introduction

The buildup of corrosion deposits known as crud, a backronym for Chalk River Unidentified Deposits, continues to pose numerous operational and safety challenges for LWR operation [1]. These deposits originate in the internal surfaces of the reactor, which may exceed 25,000 m^2 for a commercial pressurized water reactor (PWR) [2]. Although the materials which comprise the hot/cold legs (304 stainless steel) and steam generators (Alloy 600 or 690) have very slow corrosion rates at PWR conditions [3, 4], their high surface areas release a significant amount of soluble and particulate materials into the primary coolant. These corrosion products concentrate on fuel rods, especially during sub-cooled boiling or nucleate boiling, growing the porous corrosion deposits known as crud. Its porous nature leads directly to many of the issues caused by its presence, including reactor power decreases or sudden shutdowns, as recently summarized in prior publications [5, 6].

Many porous media cannot be simply described by aggregate material properties such as density, lumped thermal conductivity, or average pore size. First proposed by Mandelbrot [7], fractals or *fractalline shapes* (which display self-similar feature scaling laws, but are not true fractals) have been recognized throughout the natural and engineered world, and can better describe the complexity of many materials. Natural examples range from ocean coastlines [8], to features of rivers [9], lightning [10], soot particle geometries [11], even to foods like cauliflower and broccoli [12], snowflakes [13], and termite mounds [14]. Porous media, both natural and engineered, often display strong fractalline characteristics, such as soils [15, 16], sandstones [17, 18], sintered powder metallurgy components [19], and packed beds of spherical particles [20]. The use of these fractal dimensions, which describe the effective dimensionality of a self-similar material, more fully describe the distribution of pore or feature sizes present. Yu provides a comprehensive review of these properties and their formulas [21], which can be used to calculate bulk material properties like fluid permeability [22] which have been well-validated with experimental mea-

*Corresponding author
Email addresses: ittinop@mit.edu (I. Dumnernchanvanit), vmishra@uark.edu (V. K. Mishra), zhnq@ncepu.edu.cn (N. Q. Zhang), srobertson@transatomicpower.com (S. Robertson), adelmore@mit.edu (A. Delmore), gmota1@mit.edu (G. Mota), dhussey@epri.com (D. Hussey), wangg@westinghouse.com (G. Wang), byerswa@westinghouse.com (W. A. Byers), hereiam@mit.edu (M. P. Short)

surements [23].

The ability to predict the locations and magnitude of crud buildup, while constantly improving using industry codes like EPRI's BOA [24] and CASL's MAMBA [25] codes, is not high enough to adequately plan for its incidence. In addition, few models to date adequately treat the full complexity of a highly tortuous, porous medium like crud. More recent models of the effects of crud on critical parameters like maximum cladding temperature and critical heat flux make use of fractalline material properties [26, 27], assuming that the pore structure of crud is self-similar enough to justify the use of these structure-property correlations. Many other crud-like fouling deposits exhibit fractalline self-similarity, including biomembrane sludge [28], hematite deposits [29], salt crystallization deposits [30], and $CaCO_3$ deposits in heat exchangers experiencing boiling [31], but to date no experimental campaign has been undertaken to confirm this for PWR crud, or to determine porosity/fractal dimension scaling relationships. Knowledge of these relationships is critical, as fractal dimensions in crud are either assumed or calculated based on other parameters.

In this paper, we present experimental results verifying the fractalline properties of PWR-like fuel crud grown in a flowing PWR loop facility. The results, when compared with crud from other facilities, suggest a unifying mechanism for its formation based on the porosity-fractal dimension correlation. These results verify the main assumptions in recent models of crud effects on nuclear fuel, as well as provide a simple, measurable way to treat the complex nature of crud as a porous medium.

2. Experimental Methods

All primary SEM images, image processing scripts, accumulated data, data processing scripts, and all other information required to reproduce the results in this study can be found on our GitHub repository for this paper [32].

2.1. Specimen Preparation and Exposure

The newly constructed Internally Heated Testloop for PWRs (IHTFP) facility [33] was used for all flowing loop tests. Figure 1 shows a diagram of the IHTFP, while Table 1 shows the conditions used in the IHTFP, showing that all conditions except for Reynolds number and mass flux can be made identical to those found in PWRs. A greatly increased nanoparticulate NiO crud precursor concentration of 50.0 ppmw was used to accelerate crud growth to the days-to-weeks time frame, likely ignoring any soluble crud deposition mechanism. A pair of experiments were conducted

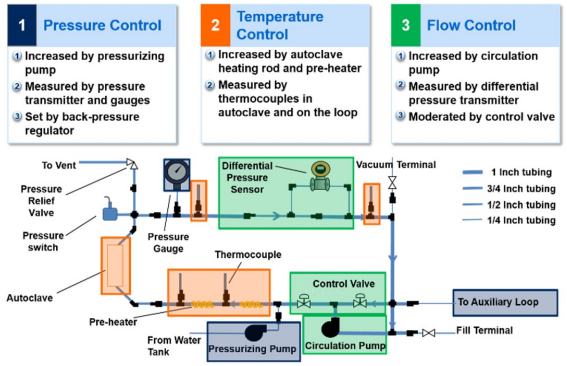

(a) Diagram of the IHTFP loop

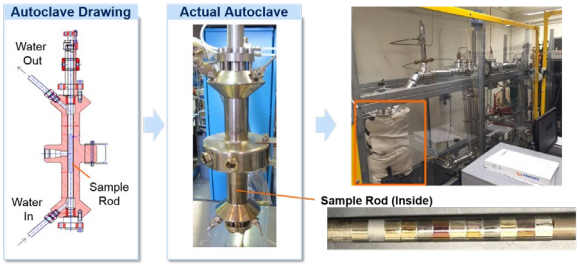

(b) Details of the autoclave (left, center) and sample mounting location (right) in the IHTFP loop

Figure 1: Diagram and images of the IHTFP flowing test loop

for nine days at these conditions, during which sub-cooled nucleate boiling induced crud deposition on ZIRLO™ substrates machined and polished to a one micron roughness. All conditions listed in Figure 1 are accurate, except that for this test a system pressure ranging from 10.3-11.5 MPa and a coolant temperature of 305-310°C resulted in a 2.7-3.1°C wall superheat according to the Thom correlation [34]. This ensure sub-cooled boiling, as evidenced by the boiling chimneys grown on the crud.

The circulation water for these experiments was mixed in a 100 liter tank connected to the circulation loop, the diagram for which is shown in Figure 1a. This was first filled with >15 MΩ/cm deionized water by evacuating the loop and using vacuum suction to draw the water in from the water storage tank, and then circulated through a mixed bed ion exchange filter and continuously measured until the water's electrical conductivity was below 0.09 μS/cm. The vacuum filling method was performed to ensure no gas bubbles would remain in the system, which would store energy when pressurized or interfere with measurement equipment. 99.999% dry argon was then bubbled through the tank until the dissolved oxygen concentration was maintained below 200 parts per billion (ppb). Then, 1,400 ppmw as B of boric acid was added to the tank, and LiOH was added until

Value	P	T (°C)	Reynolds	$G\frac{kg}{m^2 s}$	Fe_3O_4, NiO	pH	dO_2	H_3BO_3	LiOH	σ_{H_2O}
PWR	15.5 MPa	287-324	$5 \cdot 10^5$	3500	≤100 ppb	6.9-7.4	<5 ppb	0-2,000 ppm	0-5 ppm	<0.3 $\mu S/cm$
IHTFP			$1.62 \cdot 10^5$	1920	≤100 ppm					

Table 1: Conditions attainable in the IHTFP flowing PWR loop

the pH of the solution reached 7.0. This amounted to 2.2 ppmw as Li of LiOH during these tests. A Mettler-Toledo Thornton 770Max Pure Water Smart Sensor was used to measure pH, dissolved oxygen, and water conductivity. Water chemistry conditions were controlled and monitored according to the Electric Power Research Institute's (EPRI's) PWR water chemistry guidelines [35].

The IHTFP loop was heated using a combined 4,992 W of strip heaters and one vertical, internally heated, electrically isolated 1,750 W heater rod inside a windowed autoclave shown in Figure 1b, yielding a nominal heat flux of 206 kW/m² during these tests. This is lower than the PWR core average, and its suitability for growing PWR-like crud will be discussed later in this manuscript. Following flowing exposure in the IHTFP loop, the water was slowly drained from the facility, and specimens were extracted from the heater rod using a Dremel tool for scanning electron microscope (SEM) and focused ion beam (FIB) analysis. Cross sections of crud boiling chimneys and porous microstructure were created using a Zeiss NVision 40 dual-beam SEM/FIB, using successive FIB probe currents of 3 nA, 700 pA, and 80 pA to coarse-mill, clean coarse milling curtains, and clean fine milling curtains respectively for a clear image. Ten images were taken of each specimen's top-down view of the crud, and ten cross-sectional images were taken from each specimen's crud near and far away from boiling chimneys.

Flakes of loose crud were also provided from test Rod 178 from the Westinghouse Electric Company's WALT loop (355-361°C, 15.51 MPa, 977-1,940 MW/m², crud thickness of 50-130 μm). The WALT loop has already been shown to generate PWR-relevant crud [36], and it is similar to the IHTFP with the exception of a far higher heat flux due to direct ohmic heating of the simulated fuel rod, and a higher mass flux. Twenty SEM/FIB images of the WALT loop crud were also taken, to compare the IHTFP crud with that of WALT, and by extension a real PWR.

2.2. *Image Processing and Fractallinity Analysis*

SEM images of crud cross sections and top-down views were binarized using the Otsu [37] and Moment Preserving [38] threshold algorithms. In most cases, localized regions of differing contrast were corrected using adaptive image thresholding (see Figure 2a), which applies different thresholds

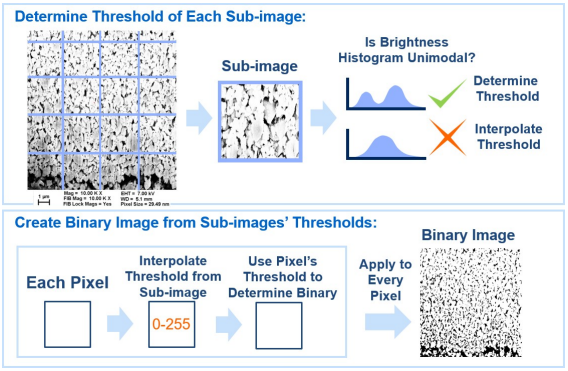

(a) Visual explanation of adaptive image processing

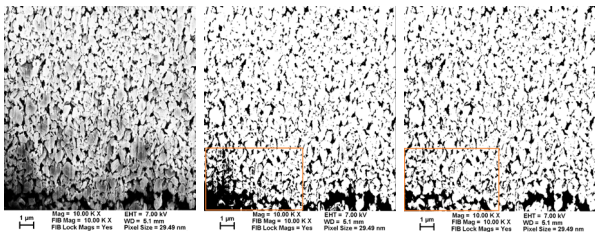

(b) Effect of normal image processing (middle) and adaptive image processing (right) on a raw SEM image of crud (left). The orange box highlights an area of particular improvement when using adaptive image processing.

Figure 2: Visual explanations of image processing techniques used to extract the fractal dimensions of crud

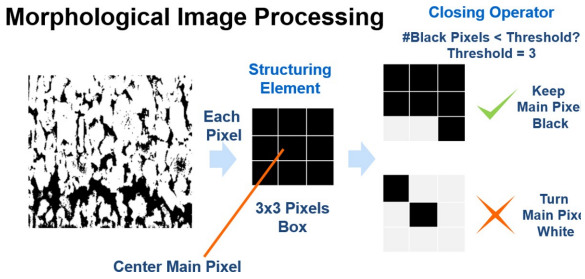

(a) Visual explanation of morphological image processing

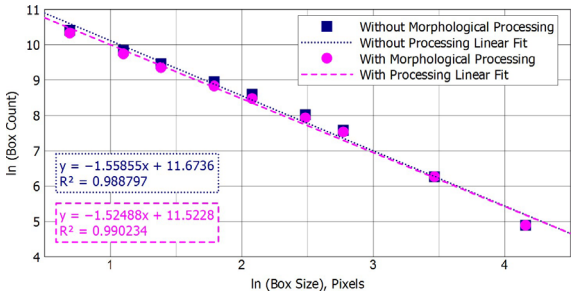

(a) Effect of morphological image processing on the fractal dimension data obtained from IHTFP crud

Figure 3: Visual explanation of morphological image processing techniques used to extract the fractal dimensions of crud and their effects on the data

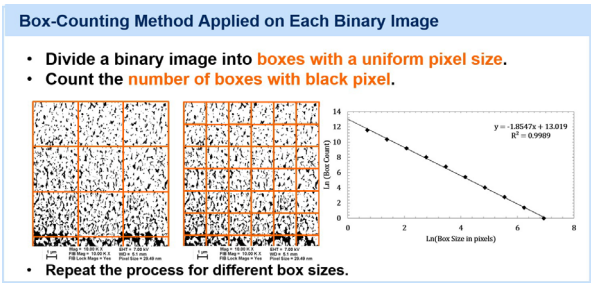

Figure 4: Illustration of the box counting method used to determine fractal dimensions of crud

to sub-images within the original images. This avoids misidentifying darker regions as pores in the crud. Finally, morphological image processing (see Figure 3a) was used to remove single-pixel artifacts due to digital noise or very small changes in contrast throughout the image, to avoid misidentifying single pixels as small pores. A subset of images obtained in this study were checked before and after morphological image processing to ensure that the final resultant fractal dimension did not change by more than 1-2%. An example of this check is shown in Figure 3b.

Processed, binarized images were then analyzed using the box counting method [39], which describes the maximum number of boxes of different sizes containing a black pixel which can be drawn on each image. Figure 4 graphically summarizes the process used, along with an example fractal dimension obtained in our study. Here, a linear best fit line is applied to the logarithmic data, yielding a power law fit. The negative slope of this trend line (the power law exponent) is the fractal dimension of this particular image. Sub-images as a function of height from the IHTFP samples were serially analyzed using the box counting method, to obtain plots of fractal dimension and porosity vs. crud thickness. As the WALT loop crud specimen was a free flake, no height could be determined, therefore the entire image was processed at once for the WALT loop specimen.

3. Results

Example images of the crud grown in these experiments are shown in Figure 5. Figure 5a shows an image of a typical ZIRLOTI' ring following two weeks of sub-cooled boiling in the IHTFP facility. The matte surface is entirely due to the formation of crud, as the specimens were shiny before entering the loop. Crud was observed to grow in similar patterns to that found in PWRs [36], with roughly 3-5 μm diameter boiling chimneys spaces 10-15 μm apart, as can be seen in Figure 5b. The machining marks visible on the sample, though very small, do appear to have helped nucleate subcooled bubbles and crud. This is actually representative of fuel surface finishes for PWR fuel cladding, as both machining and loading the fuel rods into spacer grids will leave visible scratches which can also nucleate crud. An example of how the FIB was used to isolate single boiling chimneys and their surrounding crud is shown in Figure 5c, while a cleaned cross section of one boiling chimney is shown in Figure 5d. It is from these cross sections that fractal analysis by image processing and box counting was performed.

Measured fractal dimensions from the two IHTFP experiments and the WALT loop experiment (Rod 178) are shown in Table 2. While the actual values of the fractal dimensions do vary between experiments, most notable are the high r^2 values from each log-log box counting distribution. These extremely tight correlations, never dipping below $r^2 = 0.989$, show how strongly fractalline the crud is in every case. Potential reasons for the variation in fractal dimension between experiments will be addressed next.

Relations between the height of the IHTFP crud as measured from the ZIRLOTI' cladding, its porosity, and its fractal dimension are shown in Figures 6a-6b. For thicker crud, this may vary, especially for crud that experienced a range of operating histories or fuel cycles. Each point represents the average of ten measurements in ten different, representative areas, except for the outermost point on each graph. This is because the crud varied in thickness depending on location as it often does, so

(a) As-grown crud

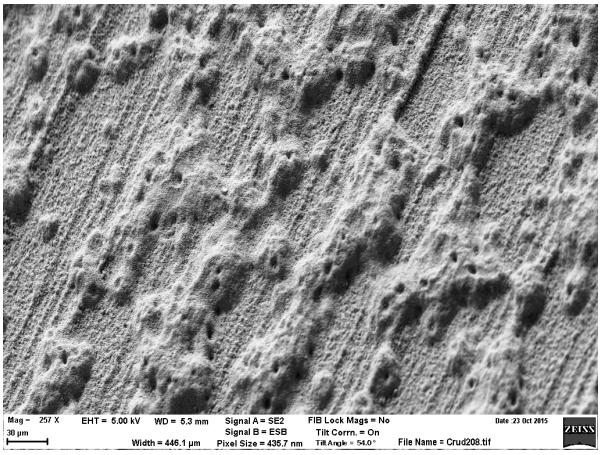

(b) Overview of crud grown in the IHTFP at PWR conditions with boiling chimneys

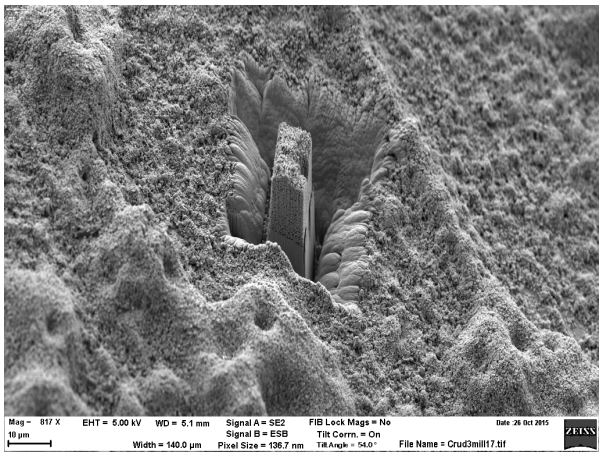

(b) FIB isolation of one boiling chimney in IHTFP crud

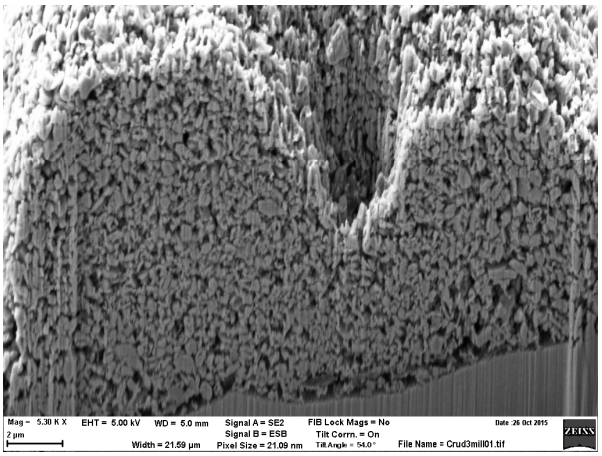

(d) FIB-milled cross section of crud boiling chimney, revealing porous microstructure for analysis

Figure 5: SEM images of the crud grown in the IHTFP facility for fractal analysis

Algorithm	**Otsu Thresholding Fractal Dimension**			
Sample	**Top View**		**Cross-Section View**	
Experiment 1	1.53 ± 0.04	r^2 = 0.995	1.51 ± 0.09	r^2 = 0.995
Experiment 2	1.38 ± 0.04	r^2 = 0.996	1.46 ± 0.08	r^2 = 0.989
WALT Rod 178	1.77 ± 0.03	r^2 = 0.998	1.61 ± 0.06	r^2 = 0.999
Algorithm	**Moment Preserving Thresholding Fractal Dimension**			
Sample	**Top View**		**Cross-Section View**	
Experiment 1	1.55 ± 0.04	r^2 = 0.995	1.53 ± 0.08	r^2 = 0.995
Experiment 2	1.40 ± 0.04	r^2 = 0.996	1.47 ± 0.08	r^2 = 0.989
WALT Rod 178	1.77 ± 0.03	r^2 = 0.998	1.61 ± 0.06	r^2 = 0.999

Table 2: Average fractal dimensions and R^2 values obtained from box-counting the crud on each sample. Errors represent one standard deviation of ten measurements per sample, per view. Two image processing algorithms, the Otsu [37] and Moment Preserving [38] thresholding techniques, are presented to show insensitivity to the binary thresholding algorithm.

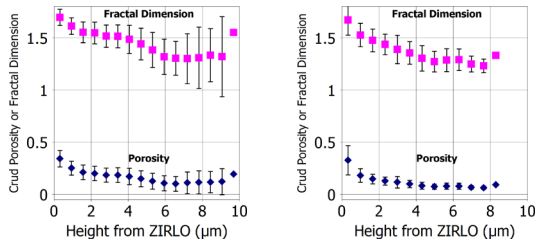

(a) Experiment 1 (b) Experiment 2

Figure 6: Relationship between crud thickness vs. porosity and fractal dimension

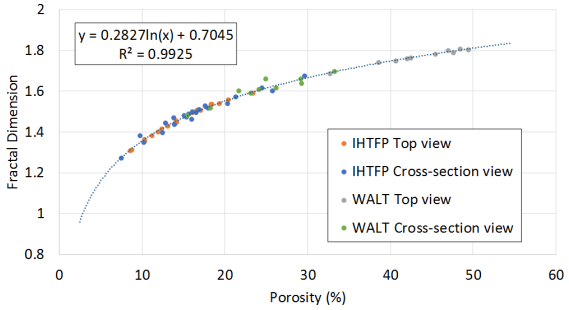

Figure 7: Relationship between porosity and fractal dimension for IHTFP and WALT crud

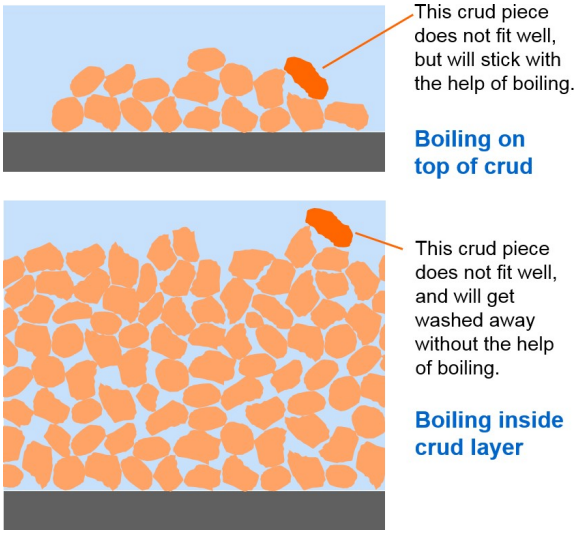

Figure 8: Proposed mechanism for decreasing porosity and fractal dimension with increasing crud thickness

fewer points were available for the outermost measurements. The data show that both crud porosity and fractal dimensions decrease with increasing crud thickness, meaning that the particles of crud are more densely packed and restrict fluid flow more severely as the crud gets thicker. Only ten microns of crud was grown during these short, two week tests, while crud in PWRs can typically reach thicknesses of 25-100 μm. It is also clear from the data in Figure 6 that crud porosity and fractal dimension are related. However, precisely how they are related determines the fractalline nature of the material, and gives clues as to how the material was formed.

The relationship between crud porosity and its fractal dimension is shown in Figure 7, combining both the IHTFP-grown and the WALT-grown crud specimens. The data follow one logarithmic trend line remarkably well, indicating significant similarities between the two specimens. While the WALT-grown crud is typically more porous than the IHTFP crud, both follow the same relationship with a very strong R^2 value of 0.9925. The reason for the higher WALT crud porosity likely stems from the significantly higher heat flux present in WALT, up to 4.5x larger, leading to a higher sub-cooled boiling rate and more rapid settling of particulate corrosion products as crud. WALT also creates crud more similar to that found in PWRs, with typical porosities ranging from 40-60%. However, because both facilities grew crud with porosity-fractal relations on the same curve, it strengthens the idea that the crud grown in IHTFP is representative of that in WALT, and by proxy in a real PWR.

4. Discussion

The results in Figures 5-7 strongly suggest that crud, like many other porous media, is a fractalline material. That does not mean that it is a truly self-similar fractal, but rather that its complex pore size distribution can be described as following self-similar scaling laws. The implications for this finding provide a simpler and more accurate way to account for the effects of crud on LWR operation, as fractal-based formulas for fluid permeability [21, 40] and thermal conductivity [41] are well established for similar porous media. The alternative is, for the example of thermal conductivity, to apply a Maxwell mixing model [42] or one of its many extensions [43] accounting for the liquid and solid phases and their volume fractions. This approach has been used in many previous models of crud thermal conductivity [44, 45, 46, 47]. Comparing a model which uses fractalline material properties [26] to a nearly identical model with simpler material property definitions [47] does indeed yield different results. Thus validating the core assumption of fractalline-based models of crud helps verify that the models are closer to correct.

The relationship between porosity, fractal dimension, and crud thickness in Figure 6 show a decreasing porosity and fractal dimension as the crud grows, when the crud is less than 10 μm thick. The development of our observed material property vs. thickness relations point to a lower boiling duty at

the top of the crud as a function of crud thickness, whereby the average particle has less of a driving force to immediately settle from intense boiling, and has more time to either find a tighter fit with other particles or be swept away by the fast moving coolant, as illustrated in Figure 8. Both of these mechanisms point to a self-limiting, slower growth rate of crud with increasing thickness with other factors held constant. This could partially explain the continuously decreasing derivative of the crud-induced power shift (CIPS) observed in PWRs [48, 49], as well as calculated saturation of crud thicknesses [5, 50].

The strong scaling behavior seen in both crud growth facilities suggests that similar mechanisms are at play in the creation of crud, and therefore its expected effects on PWR fuel cladding. This means that a simpler porosity measurement of crud can lead directly to its fractal dimensions given growth in PWR conditions, allowing for more rapid and accurate estimation of its effect on fuel performance. This scaling behavior is seen in numerous other systems, where the relationship between porosity and fractal dimension reveals the type and growth conditions of the porous medium. For example, De Gryze et al found different fractal dimension scaling laws for two types of soil, sandy loam and silt loam, and for different soil ages [16], while Dathe and Thuller found a strong relationship between porosity and fractal dimension in soil [15]. Yu and Li find somewhat differentiable porosity/fractal scaling laws for differently woven and dispersed fiber composites [51], while Tang et al report rather different curves for sintered stainless steel components [19].

5. Conclusions

The porous reactor corrosion deposits known as crud were shown to be fractalline in nature through electron microscopy and image processing analysis. The porosity vs. fractal dimension scales remarkably well, including with other PWR-like loop facilities, suggesting that the results here are representative of those found in a PWR. Results suggest that not only can post-mortem analysis of crud fractal dimensions be used to estimate its effects on fuel cladding, but also that changes in the fractal dimensions can indicate effectiveness in anti-fouling measures taken to ameliorate the growth and effects of crud [31]. Measured fractal dimensions can seamlessly be inserted into codes like MAMBA-BDM [26] with spatial dependence, or into industry codes like BOA using the porosity-fractal dimension scaling laws found in this study.

Acknowledgments

Particular thanks are due to the Electric Power Research Institute (EPRI), for funding this work from its inception through loop testing under their Polaris and PWR Technical Advisory Committee (P-TAC) programs on contract numbers 10002739, 10004433, and 10005086. Thanks are also due to the MIT Center for Advanced Nuclear Energy Systems (CANES), an MIT Energy Initiative (MITEI) Low-Carbon Energy Center (LCEC), for providing support for the loop testing autoclave, and to the MIT-Japan Hayashi Seed Grant for providing seed funds for this work. The authors also thank Kevin Harding of the Westinghouse Electric Company LLC for his work running and maintaining the WALT loop, and Peter Stahle of MIT for helping with the construction and maintenance of the IHTFP loop.

References

[1] P. L. Frattini, J. Blok, S. Chauffriat, J. Sawicki, and J. Riddle. Axial offset anomaly: coupling PWR primary chemistry with core design. *Nucl. Ener.*, 40(2):123–135, 2001.

[2] A. Kunkle and D. Testa. The westinghouse pressurized water reactor nuclear power plant. Technical report, Westinghouse Electric Division, 1984. Accessed at http://www4.ncsu.edu/ doster/ NE405/Manuals/PWR Manual.pdf on 2017-04-30.

[3] F. Carrette, M. C. Lafont, G. Chatainier, L. Guinard, and B. Pieraggi. Analysis and TEM examination of corrosion scales grown on alloy 690 exposed to pressurized water at 325 C. *Surf. Interface Anal.*, 34(1):135–138, 2002.

[4] R. Molins, M. Pijolat, M. Sennour, L. Marchetti, S. Perrin, and O. Raquet. Characterization of the oxide films formed at the surface of Ni-base alloys in pressurized water reactors primary coolant by transmission electron microscopy. *Mater. Sci. Forum*, 595:539–547, 2008.

[5] J. Deshon, D. Hussey, B. Kendrick, J. McGurk, J. Secker, and M. P. Short. Pressurized water reactor fuel crud and corrosion modeling. *JOM*, 63(8):64, 2011.

[6] I. Dumnernchanvanit, N. Q. Ziang, S. Robertson, A. Delmore, M. B. Carlson, D. Hussey, and M. P. Short. Initial experimental evaluation of crud-resistant materials for light water reactors. *J. Nucl. Mater.*, 2017. DOI: 10.1016/j.jnucmat.2017.10.010.

[7] B. B. Mandelbrot. *The Fractal Geometry of Nature*. International Business Machines (IBM), 1983.

[8] J. W. Jiang and R. E. Plotnick. Fractal analysis of the complexity of United States coastlines. *Mathematical Geol.*, 30(5):535–546, 1998.

[9] D. G. Tarboton, R. L. Bras, and I. Rodriguez-Iturbe. The fractal nature of river networks. *Water Resour. Res.*, 24(8):1317–1322, 1988.

[10] J. Sañudo, J. B. Gómez, F. Castaño, and A. F. Pacheco. Fractal dimension of lightning discharge. *Nonlinear Processes in Geophysics*, 2:101–106, 1995.

[11] Ü. Ö. Köylü, G. M. Faeth, T. L. Farias, and M. G. Carvalho. Fractal and projected structure properties of soot aggregates. *Combust. Flame*, 100(4):621–633, 1995.

[12] M. Peleg and G. V. Barbosa. Fractals and foods. *Crit. Rev. Food Sci. Nutr.*, 33(2):149–165, 1993.

[13] P. S. Addison. *Fractals and Chaos: An illustrated course*. Institute of Physics Publishing, 1997.

[14] N. Y. Su and H. Puche. Tunneling activity of subterranean termites (isoptera: Rhinotermitidae) in sand with moisture gradients. *J. Econ. Entomol.*, 96(1):88–93, 2003.

[15] A. Dathe and M. Thullner. The relationship between fractal properties of solid matrix and pore space in porous media. *Geoderma*, 129(3-4):279–290, 2005.

[16] S. De Gryze, L. Jassogne, J. Six, H. Bossuyt, M. Wevers, and R. Merckx. Pore structure changes during decomposition of fresh residue: X-ray tomography analyses. *Geoderma*, 134(1-2):82–96, 2006.

[17] A. J. Katz and A. H. Thompson. Fractal sandstone pores: Implications for conductivity and pore formation. *Phys. Rev. Lett.*, 54:1325–1328, 1985.

[18] C. E. Krohn and A. H. Thompson. Fractal sandstone pores: Automated measurements using scanning-electron-microscope images. *Phys. Rev. B*, 33:6366–6374, 1986.

[19] H. P. Tang, J. Z. Wang, J. L. Zhu, Q. B. Ao, J. Y. Wang, B. J. Yang, and Y. N. Li. Fractal dimension of pore-structure of porous metal materials made by stainless steel powder. *Powder Technol.*, 217:383–387, 2012.

[20] C. A. Baldwin, A. J. Sederman, M. D. Mantle, P. Alexander, and L. F. Gladden. Determination and characterization of the structure of a pore space from 3D volume images. *J. Colloid Interface Sci.*, 181(1):79 – 92, 1996.

[21] B. M. Yu. Analysis of flow in fractal porous media. *Appl. Mech. Rev.*, 61(5):050801, 2008.

[22] B. M. Yu and W. Liu. Fractal analysis of permeabilities for porous media. *AIChE J.*, 50(1):46–57, 2004.

[23] H. Pape, C. Clauser, and J. Iffland. Permeability prediction based on fractal pore-space geometry. *Geophys.*, 64(5):1447–1460, 1999.

[24] EPRI. Boron-induced offset anomaly (BOA) risk assessment tool, version 1.0. Technical Report 1003211, Electric Power Research Institute (EPRI), Palo Alto, CA, USA, 2003.

[25] V. Petrov, B. K. Kendrick, D. Walter, A. Manera, and J. Secker. Prediction of CRUD deposition on PWR fuel using a state-of-the-art CFD-based multiphysics computational tool. *Nucl. Eng. Des.*, 299:95–104, 2016.

[26] M. M. Jin and M. P. Short. Multiphysics modeling of two-phase film boiling within porous corrosion deposits. *J. Comput. Phys.*, 316:504–518, 2016.

[27] D. Y. Yeo and H. C. No. Modeling heat transfer through chimney-structured porous deposit formed in pressurized water reactors. *Intl. J. Heat Mass Trans.*, 108, Part A:868–879, 2017.

[28] F. G. Meng, H. M. Zhang, Y. S. Li, X. W. Zhang, F. L. Yang, and J. N. Xiao. Cake layer morphology in microfiltration of activated sludge wastewater based on fractal analysis. *Sep. Purif. Technol.*, 44(3):250–257, 2005.

[29] T. D. Waite, A. I. Schäfer, A. G. Fane, and A. Heuer. Colloidal fouling of ultrafiltration membranes: Impact of aggregate structure and size. *J. Colloid Interface Sci.*, 212(2):264–274, 1999.

[30] A. Helalizadeh, H. Müller-Steinhagen, and M. Jamialahmadi. Mixed salt crystallisation fouling. *Chem. Eng. Process.: Process Intensification*, 39(1):29–43, 2000.

[31] Q. F. Yang, Y. Q. Liu, A. Z. Gu, J. D., and Z. Q. Shen. Investigation of induction period and morphology of CaCO3 fouling on heated surface. *Chem. Eng. Sci.*, 57(6):921–931, 2002.

[32] [Dataset] I. Dumnernchanvanit, N. Q. Zhang, S. Robertson, A. Delmore, M. B. Carlson, D. Hussey, and M. P. Short. Data and code/script repository for 2017 IHTFP fractalline crud paper, 2017. GitHub repository. Accessible at https://github.com/shortlab/ Permanent Link at DOI: 10.5281/zenodo.854694.

[33] I. Dumnernchanvanit, N. Zhang, A. R. Delmore, and M. P. Short. Design and assembly of experimental facility for CRUD characterization and mitigation at PWR cladding conditions. *Trans. Amer. Nucl. Soc.*, 111:1579–1582, 2014.

[34] N. E. Todreas and M. S. Kazimi. *Nuclear Systems I: Thermal Hydraulic Fundamentals*. Taylor & Francis, 1990.

[35] J. Deshon et al. Pressurized water reactor primary water chemistry guidelines: Revision 7, volumes 1 and 2. Technical Report 3002000505, Electric Power Research Institute (EPRI), Palo Alto, CA, USA, 2014.

[36] J. Deshon. Simulated fuel crud thermal conductivity measurements under pressurized water reactor conditions. Technical report, EPRI, 2011. Tech. Rep. 1022896.

[37] N. Otsu. A threshold selection method from gray-level histograms. *IEEE Trans. Sys., Man., Cyber.*, 9(1):62–66, 1979.

[38] W.-H. Tsai. Moment-preserving thresholding: a new approach. *Computer Vision Graphics and Image Processing*, 19:377–393, 1984.

[39] R. Lopes and N. Betrouni. Fractal and multifractal analysis: a review. *Med. Image Anal.*, 13(4):634–649, 2009.

[40] R. Pitchumani and B. Ramakrishnan. A fractal geometry model for evaluating permeabilities of porous preforms used in liquid composite molding. *Intl. J. Heat Mass Trans.*, 42(12):2219–2232, 1999.

[41] Y. Shi, J. Xiao, S. Quan, M. Pan, and R. Yuan. Fractal model for prediction of effective thermal conductivity of gas diffusion layer in proton exchange membrane fuel cell. *J. Power Sources*, 185(1):241–247, 2008.

[42] J. C. Maxwell. *Treatise on Electricity and Magnetism*. Clarendon Press, Oxford, UK, 1873.

[43] W. H. Yu, D. M. France, J. L. Routbort, and S. U. S. Choi. Review and comparison of nanofluid thermal conductivity and heat transfer enhancements. *Heat Transfer Eng.*, 29(5):432–460, 2008.

[44] P. Cohen. Heat and mass transfer for boiling in porous deposits with chimneys. *AIChE Symp. Ser.*, 70:71, 1974.

[45] C. Pan, B. G. Jones, and A. J. Machiels. Concentration levels of solutes in porous deposits with chimneys under wick boiling conditions. *Nucl. Eng. Des.*, 99:317–327, 1987.

[46] J. Henshaw, J. C. McGurk, H. E. Sims, A. Tuson, S. Dickinson, and J. Deshon. A model of chemistry and thermal hydraulics in PWR fuel crud deposits. *J. Nucl. Mater.*, 353(1-2):1–11, 2006.

[47] I. ul Haq, N. Cinosi, M. Bluck, G. Hewitt, and S. Walker. Modelling heat transfer and dissolved species concentrations within PWR crud. *Nucl. Eng. Des.*, 241(1):155–162, 2011.

[48] J. Deshon et al. PWR axial offset anomaly (AOA) guidelines, revision 1. Technical Report 1008102, Electric Power Research Institute (EPRI), Palo Alto, CA, 2004.

[49] E. Decossin and K. Fruzzetti. Modeling the axial offset of two cycles of a 900-MW pressurized water reactor core. Technical report, Electric Power Research Institute (EPRI), 2006. Tech. Rep. 1013681.

[50] D. J. Walter, B. K. Kendrick, V. Petrov, A. Manera, B. Collins, and T. Downar. Proof-of-principle of high-fidelity coupled CRUD deposition and cycle depletion simulation. *Ann. Nucl. Energy*, 85:1152–1166, 2015.

[51] B. M. Yu and J. H. Li. Some fractal characters of porous media. *Fractals*, 9(3):365–372, 2001.